Cell

The Molecular Diversity of *Dscam* Is Functionally Required for Neuronal Wiring Specificity in *Drosophila*

Brian E. Chen,[1,2] Masahiro Kondo,[1,2] Amélie Garnier,[1] Fiona L. Watson,[1] Roland Püettmann-Holgado,[1] David R. Lamar,[1,3] and Dietmar Schmucker[1,*]
[1] Department of Cancer Biology, Dana-Farber Cancer Institute, Department of Neurobiology, Harvard Medical School, Boston, MA 02115, USA
[2] These authors contributed equally to this work.
[3] Present address: Department of Medicine, Emory University School of Medicine, Atlanta, GA 30322, USA
*Contact: dietmar_schmucker@dfci.harvard.edu
DOI 10.1016/j.cell.2006.03.034

SUMMARY

Alternative splicing of *Dscam* generates an enormous molecular diversity with maximally 38,016 different receptors. Whether this large diversity is required in vivo is currently unclear. We examined the role of Dscam in neuron-target recognition of single mechanosensory neurons, which connect with different target cells through multiple axonal branches. Analysis of Dscam null neurons demonstrated an essential role of Dscam for growth and directed extension of axon branches. Expression of randomly chosen single isoforms could not rescue connectivity but did restore basic axonal extension and rudimentary branching. Moreover, two Dscam alleles were generated that each reduced the maximally possible Dscam diversity to 22,176 isoforms. Reduction of Dscam diversity resulted in specific connectivity defects of mechanosensory neurons. Furthermore, the observed allele-specific phenotypes suggest functional differences among isoforms. Our findings provide evidence that a very large number of structurally unique receptor isoforms is required to ensure fidelity and precision of neuronal connectivity.

INTRODUCTION

The specific connectivity of axons and dendrites is the functional foundation of the nervous system and can be thought of as emerging in distinct steps: outgrowth and guidance of neuronal processes to a target field, choice of the appropriate target from within the local environment, and finally the assembly of synapses at distinct subcellular compartments (reviewed in Tessier-Lavigne and Goodman, 1996; Benson et al., 2001; Huber et al., 2003). The mechanisms underlying target recognition and specific synapse formation are not well understood. In particular, molecular interactions that regulate contact with multiple targets and control the restrictions of synaptic contacts to layers or laminae as well as subcellular compartments are largely unknown (Yamagata et al., 2002; Ango et al., 2004).

Roger Sperry proposed in the chemo-affinity hypothesis that an axon will link up to a postsynaptic target by selective attachment mediated by specific chemical affinities (Sperry, 1963). He pointed out that the high degree of specificity implicit in this hypothesis required invoking either an enormous number of different molecular labels (chemical affinities) or the ability of an integrative graded response to different concentrations of a small number of signals. The work of many groups has established that complementary gradients of Eph receptors and their ligands are an important example of the latter possibility (Cheng et al., 1995; Flanagan and Vanderhaeghen, 1998; Hindges et al., 2002). Although gradients of diffusible signals and their complementary receptors provide mechanisms for the guidance of axons during topographic map formation, many questions remain regarding other guidance mechanisms, local target selection, and synapse specification.

In the olfactory system, it has been proposed that the molecular diversity provided by the large gene family (~1000) of olfactory receptors (OR) plays an instructive role in connection specificity (Wang et al., 1998; Vassalli et al., 2002; Feinstein and Mombaerts, 2004). Each one of the millions of olfactory neurons expresses only a single OR, and axons expressing the same receptor coalesce and form connections with single glomeruli. Receptor-swap experiments have shown that changing only a small number of amino acids in an OR is sufficient to respecify the target selection of the olfactory neurons expressing these modified ORs (Feinstein and Mombaerts, 2004). ORs are expressed only in olfactory neurons, and it remains unclear whether different diverse receptors will show a similar ability in regulating targeting specificity in other regions of the central nervous system.

Other gene families of neural receptors capable of generating a large molecular diversity have been identified. These include neurexins (Missler et al., 1998), cadherins (reviewed in Takeichi et al., 1997), and cadherin-related neuronal receptors (CNRs) (Kohmura, et al., 1998; Uemura, 1998; Wu and Maniatis, 1999). Recent genetic analyses of the neurexin and CNR gene clusters have demonstrated their importance in synapse development (Boucard et al., 2005; Weiner et al., 2005). In addition, a substantial number of diverse immune receptors are expressed in the mammalian brain (reviewed in Boulanger and Shatz, 2004), and for the MHC-class of receptors it has been shown that they are functionally required for synaptic specificity (Huh et al., 2000).

The *Drosophila* gene *Dscam* has been proposed to function as an important regulator of synaptic specificity because of its extraordinary molecular diversity. *Drosophila Dscam* can potentially generate 38,016 different mRNA isoforms through alternative splicing (Schmucker et al., 2000). This unprecedented number of unique receptor isoforms could be used to distinguish both cell and even synapse identities through selective expression and localization. Dscam protein is required throughout the developing nervous system for many aspects of axon guidance, targeting, axon branch specification, and dendrite patterning (Schmucker et al., 2000; Wang et al., 2002; Hummel et al., 2003; Wang et al., 2004; Zhan et al., 2004; Zhu et al., 2006). PCR-based expression studies have suggested that the Dscam repertoire of each cell is different from those of its neighbors and may be utilized to generate unique cell identities in the nervous system (Neves et al., 2004). Furthermore, in vitro binding studies have shown that Dscam isoforms can interact in a highly selective homophilic manner where even closely related isoforms show little interaction and exhibit almost exclusive isoform-specific binding (Wojtowicz et al., 2004).

However, genetic analysis of Dscam has not provided conclusive evidence for the requirement of Dscam diversity in specifying neuronal connectivity. Previous experiments have shown that single Dscam isoforms could rescue defects in Dscam null mushroom body neurons during neuronal differentiation or axon bifurcation. Different isoforms rescued the phenotypic defects equally well, questioning the need for the molecular diversity of Dscam in this system (Wang et al., 2004; Zhan et al., 2004).

Here we present a systematic analysis of Dscam function in the precise targeting of axon branches within the somatosensory system of flies. First, our study identifies an essential function of Dscam for branching and targeting of mechanosensory neurons. Second, we find that expression of different single Dscam isoforms in Dscam null neurons rescues primary axonal branch extension and rudimentary branching but does not rescue the specific targeting of axonal branches. Third, Dscam mutant flies expressing only a reduced subset of 22,176 possible isoforms show specific axon targeting errors or deviations in nearly all of the mutant flies. Fourth, comparisons of axonal targeting errors between mutant flies revealed distinguishable phenotypes in flies that lack different subsets of isoforms. This supports the hypothesis that the molecular diversity of Dscam receptors is required for establishing the precise connections of a *Drosophila* sensory circuit and raises the possibility that local isoform-specific interactions instruct axonal branches to connect with their proper targets.

RESULTS

Single-Cell Analysis of Axon Branching and Targeting in the CNS of Adult Flies

To determine the role of specific isoforms in axonal targeting, an experimental system was chosen in which "general" versus isoform-specific Dscam functions could be distinguished. To this end we characterized the normal axonal targeting of adult mechanosensory neurons (ms-neurons) within the *Drosophila* somatosensory system. We focused on ms-neurons that innervate large bristles, or macrochaetae, of the posterior thorax, which sense airflow and touch (Figure 1). The axonal targeting of these ms-neurons is remarkably precise where much of the synaptic connectivity is invariant, and afferent projections of each ms-neuron are recognizable by their stereotyped axonal branching pattern within the Central Nervous System (CNS) (Ghysen, 1978; Canal et al., 1998; Grillenzoni et al., 1998; Williams and Shepherd, 2002). Thirteen symmetrical pairs of macrochaetae and their associated ms-neurons are situated on opposite sides of the posterior thorax in stereotyped positions. Thus, the same ms-neuron can be identified in different animals by its specific corresponding bristle (Figures 1A and 1B). Ms-neurons situated at different body positions exhibit characteristic branching patterns. Therefore, the axonal branching pattern of ms-neurons can be used as a morphological readout for neuron-specific differences in connectivity (Canal et al., 1998).

To trace the axonal projections of single ms-neurons, two experimental methods were combined. The MARCM system (Lee and Luo, 1999) was used to generate mosaic animals that express GFP in a small number of ms-neurons (Figure 1B and Experimental Procedures). Heatshock-mediated induction of Flp-recombinase resulted in stochastically occurring mosaic clones as indicated by GFP expression in ms-neurons (Figure 1B). To achieve exclusive single axon resolution and equal staining throughout axonal branches, we used anterograde labeling with lipophilic fluorescent dyes such as DiI and DiD (Experimental Procedures). Ms-neurons labeled by GFP, lipophilic dye, or both were selected, and axonal projections and arborizations within the thoracic ganglia were imaged. We examined the posterior Dorsocentral, (pDc), anterior Scutellar (aSc), and posterior Scutellar (pSc) neurons. In order to determine the invariant and variable aspects of the axonal branching pattern in wild-type animals, we conducted a quantitative analysis of the pSc projections (Figure 1D). The lengths and positions of the primary and secondary axonal branches in 41 wild-type flies were measured (Experimental Procedures). Eleven axonal branches were

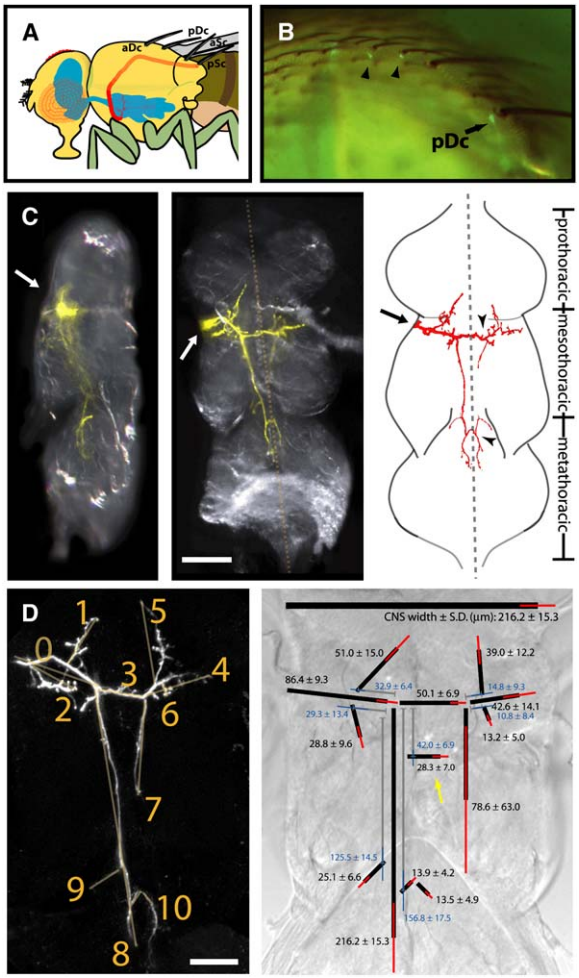

Figure 1. Analysis of Neuronal Connectivity in the Adult *Drosophila* Somatosensory System at Single Axon Resolution Using MARCM and Dye-Labeling

(A) Schematic of the axon trajectory of a single mechanosensory neuron. Four mechanosensory bristles are shown: aDc, pDc, aSc, and pSc with its corresponding ms-neuron and axonal branching pattern (red) within the CNS (blue).

(B) Each bristle is innervated by a single ms-neuron. Side view of an adult thorax and with a single GFP-labeled pDc neuron (arrow) situated below its corresponding macrochaeta. Additional ms-neurons associated with microchaetae (arrowheads) indicate additional clones and are also GFP-labeled.

(C) Mechanosensory axons extend complex arbors within the thoracic ganglion. Lateral (left) and ventral (middle) views of the thoracic ganglion with a single pSc axon labeled. The thoracic ganglion comprises three distinct segments, with prothoracic, mesothoracic, and metathoracic neuromeres (right image, schematic). Ms-axons enter the CNS between the prothoracic and mesothoracic neuromeres (arrows). The pSc axon extends its arbor within all three segments and has two contralateral projecting secondary branches (arrowheads). Dotted lines mark the midline of the CNS.

(D) Analysis of axon branch length and position in pSc neurons. Left: Lengths of the axonal branches of the posterior pSc neuron in wild-type flies were measured. Eleven primary and secondary branches constitute the prototypic branching pattern. Right: Average lengths and positions of primary and secondary branches of the wild-type pSc neurons. Black lines represent the average lengths with standard deviations in red. Gray lines represent average positions of branches with standard deviations in blue. All numbers are in micrometers. Arrow denotes an ectopic branch in wild-type flies. Scale bars = 50 μm.

detectable at 99.5% frequency and were therefore designated as a prototypic pSc branching pattern. A single branch at a mesothoracic position occurred at low frequency (12%) and was therefore designated as an ectopic branch (Figure 1D). A large variance in the length of an axonal branch was found for the contralateral, descending secondary branch (Figure 1D). All other branches showed significantly less variation in axon length and relative position.

Dscam Function Is Essential for Axonal Targeting of Mechanosensory Neurons

We next analyzed the axonal projections of Dscam mutant neurons. Mosaic animals were generated in which a small subset of ms-neurons were homozygous for strong loss of function alleles of Dscam (Dscam^{20}, Dscam^{21}, or Dscam^{33}) (Experimental Procedures). Nearly all Dscam mutant axons reached the CNS and entered the thoracic ganglion correctly, between the pro- and mesothoracic neuromeres (Figure 2). Within the CNS, however, all of the Dscam null ms-axons failed to elaborate any branches that connect to different targets (Figures 2B, 2C, and 2E–2J). The absence of Dscam within ms-axons does not appear to simply inhibit axonal branch formation (Figure 2I), as distinct axonal branches are still recognizable but remain tightly clustered in a small (<20 μm) bolus around a presumptive decision point. These phenotypic abnormalities suggest that nascent axonal branches fail to project away from the main axon shaft and are unable to extend in the appropriate directions. The characteristic targeting failure occurred at 100% penetrance in all Dscam null ms-neurons tested (n = 112), regardless of the type of ms-neuron (pDc, aSc, or pSc) analyzed (Figure 2J). It is likely that Dscam is required in the sensory neuron as well as in the CNS target area, and defects in the CNS could also have contributed to the observed targeting defects. To address this possibility, an analysis was carried out directly comparing the projections of Dscam heterozygous and homozygous null ms-axons encountering the same mosaic CNS target area (Supplemental Data and Figure S1). These experiments also provided support for an important cell-autonomous function of Dscam within ms-neurons. We conclude that Dscam expression within ms-neurons is essential for the establishment of the connectivity of axonal branches but dispensable for axon guidance from the periphery into the CNS.

Dscam cDNAs of Single Isoforms Cannot Rescue Specific Axonal Targeting but Reveal a Basic Function of Dscam for Axon Extension

We next investigated whether different Dscam isoforms fulfill distinguishable functions during axonal targeting. Transgenic flies were generated bearing UAS-*Dscam* constructs of three isoforms obtained from mRNAs expressed

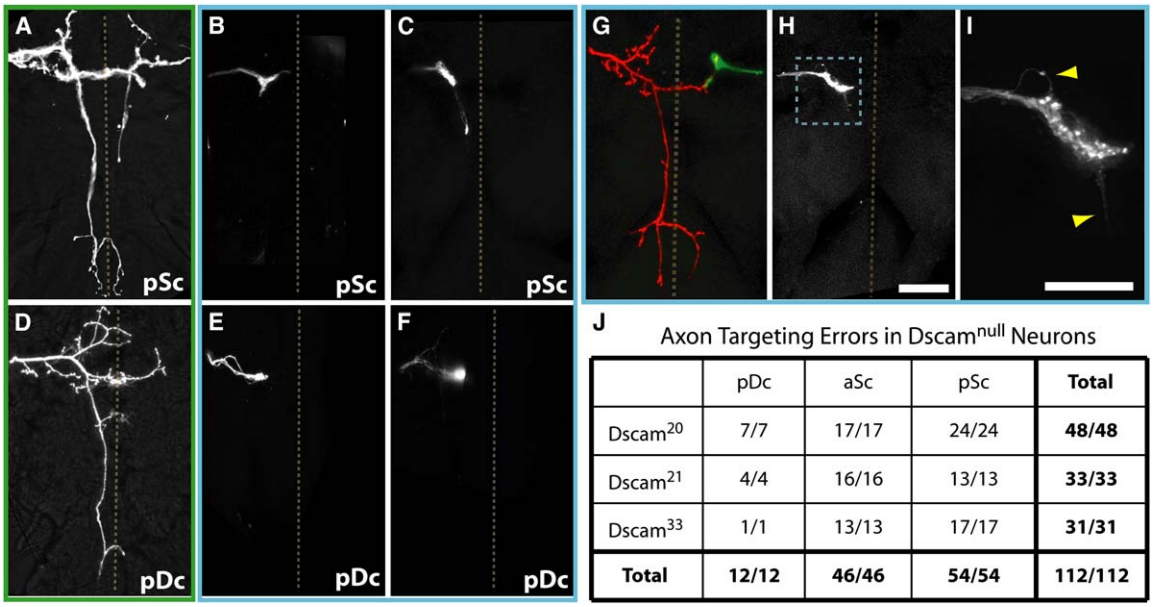

	pDc	aSc	pSc	Total
Dscam^{20}	7/7	17/17	24/24	**48/48**
Dscam^{21}	4/4	16/16	13/13	**33/33**
Dscam^{33}	1/1	13/13	17/17	**31/31**
Total	**12/12**	**46/46**	**54/54**	**112/112**

Figure 2. The Axon Guidance Receptor Dscam Is Required for Axonal Connectivity of ms-neurons within the CNS but Not for the Initial Pathfinding

(A and D) Different ms-neurons form unique branching patterns within the CNS. Primary and secondary axon branches of the pSc (A) and pDc (D) ms-neurons in wild-type flies connect with different cells.

(B, C, E, and F) Dscam is essential for targeting of axonal branches, and ms-neurons that are null for Dscam fail to elaborate any arbors. Representative examples for pSc (B and C) and pDc (E and F) projections are shown.

(G) Axonal projection of a heterozygous pSc neuron (red, left side) exhibiting normal branching pattern. In contrast, a pSc neuron lacking Dscam (green, right side) failed to elaborate axonal branches. A homozygous Dscam^{20} (GFP-positive) ms-neuron and a neighboring heterozygous Dscam$^{20/+}$ (GFP-negative) ms-neuron were labeled with different fluorescent dyes in the same animal. Note the homozygous Dscam null neuron (green axon, right) enters the thoracic ganglion at the correct position but does not contact any targets. The contralateral ms-neuron containing Dscam (red axon, left) branches appropriately.

(H and I) Dscam null neurons fail to extend axonal branches toward appropriate targets. Nevertheless, a Dscam null ms-neuron is able to form axonal branches (arrowheads) and bears varicosities but does not extend branches away from the "decision point." Scale bars for (A)–(H) = 50 μm; for (I) = 25 μm.

(J) Axon targeting errors in Dscam null neurons occur at 100% penetrance. All ms-neurons and all *Dscam^{LOF}* alleles tested fail to contact any appropriate targets.

Table 1. Frequency of pSc Axonal Branching Errors among Different Genotypes

		Group 1			
Genotype	n	Total Group1 Errors	Ectopic Branch	Ectopic Midline-Crossing Branch	Contralateral Branch Extension
+/+	81	0%	0%	0%	0%
Dscam$^{\Delta R265}$/Dscam$^{\Delta R265}$	66	27.9%	13.8%	6.2%	6.3%
Dscam$^{\Delta R265}$/Dscam^{null}	34	26.8%	20.6%	2.9%	0%
Dscam$^{\Delta R265}$/+	54	6.1%	1.9%	1.9%	2.3%
Dscam$^{\Delta R272}$/ Dscam$^{\Delta R272}$	56	34.6%	3.6%	1.8%	12.5%
Dscam$^{\Delta R272}$/Dscam^{null}	43	19.5%	2.3%	0%	10.3%
Dscam$^{\Delta R272}$/+	44	7.3%	4.5%	0%	0%
Dscam$^{\Delta R265}$/ Dscam$^{\Delta R272}$	36	20.5%	8.3%	5.6%	3.3%
Dscam^{null}/+	81	8.3%	1.2%	0%	0%

Targeting phenotypes were classified into two groups: Group 1, targeting errors never observed in wild-type flies; and Group 2, variable targeting phenotypes that occurred in wild-type flies at low frequency. The frequency of flies having each axonal error is indicated in each column below the schematic of the error; targeting errors are not mutually exclusive. The Total Group 1 Errors column summarizes all Group 1 errors. Schematic depiction of phenotypic grouping is given in Table S1.

in the developing nervous system (A = 1.30.30.2; B = 1.34.30.2; C = 7.6.19.2) (Experimental Procedures). Specific expression of Dscam isoforms within aSc or pSc neurons is presently unknown, and it is unclear whether they endogenously express isoforms A, B, or C. Nevertheless, all three isoforms contain the transmembrane segment encoded by exon 17.2, which has been reported to be important for localization to axons and is essential for rescue of axonal phenotypes in the adult mushroom body (Wang et al., 2004; Zhan et al., 2004). Two independent transgene insertions of isoforms B and C and one of isoform A were tested for rescue of ms-neurons. Clones of Dscam null mutant cells were generated by MARCM, where selective loss of the GAL80 repressor allows for the GAL4-driven expression of both UAS-*Dscam* and UAS-mCD8-GFP under the control of the pan-neuronal promoter *elav* (Experimental Procedures). The axonal projections of 32 single ms-neurons, which included pDc, aSc, and pSc neurons, were analyzed (Figure 3).

Single isoform expression in ms-neurons could only partially rescue Dscam loss-of-function phenotypes. Ms-neurons that lacked all Dscam protein characteristically could not grow secondary or tertiary branches, and a thin, short extension was occasionally observed (Figures 2C and 3B). In contrast, ms-neurons that expressed a single Dscam isoform showed a substantial rescue of the axon extension into the posterior compartments of the CNS (Figures 3C–3E and 3I–3K). However, specific axon extension in the anterior direction and especially to the contralateral side was mostly absent in neurons expressing only a single isoform. Only a single sample revealed the presence of a branch extending across the midline within the mesothoracic segment, where it stopped without forming any tertiary branches (Figure 3K).

We analyzed the ms-neuron phenotypes of aSc and pSc neurons, which have a highly similar branching pattern in wild-type flies, and found that expression of isoform A was able to rescue the anterior branch extension in three out of four animals but could not rescue the contralateral projection (Figure 3C and 3I). In contrast, expression of isoform C entirely failed to rescue the anterior branch extension (0/6). In order to address whether an increase in Dscam expression would improve the rescue of ms-neurons, experiments were performed in which the transgene copy number had been doubled. However, no improvements of rescue in neurons expressing two copies of isoform B or C compared to single-copy rescues were detected (Figures 3F, 3L, and 3R). A significant increase in Dscam activity was verified using a dominant gain of function assay (Figure S2). Therefore, the lack of rescue of anterior or contralateral branches is not likely due to low Dscam protein expression.

Taken together, these experiments suggest that a "core" activity of Dscam is necessary to facilitate axon extension of ms-neurons within the CNS and that this activity can be rescued equally well by different isoforms. In contrast, specific aspects of targeting, such as position or number of branches and directed branch extension, may require specific isoforms or combinations of isoforms.

Dscam$^{\Delta R265}$ and *Dscam*$^{\Delta R272}$ Are Alleles with Reduced Isoform Diversity but Normal Dscam mRNA and Protein Levels

The rescue experiments using cDNAs of single isoforms suggest that different isoforms might be utilized in vivo for distinct branching or targeting decisions. However, given the large number of Dscam isoforms and substantial technical difficulties, isoform rescue experiments do not

Table 1. (Continued)

Group 1			Group 2				
Ipsilateral Branch Extension	Truncated Posterior Branch	Uncategorizable	Ectopic Branch	Inverted Branch Order	Ectopic Midline Branch	Incomplete Midline-Crossing Branch	No Midline-Crossing Branch
0%	0%	0%	15.6%	3.3%	11.5%	6.6%	3.3%
0%	0%	1.6%	70.1%	12.7%	12.7%	12.7%	1.6%
0%	0%	3.3%	51.6%	10.0%	23.3%	13.3%	20.0%
0%	0%	0%	34.0%	11.6%	16.3%	18.6%	2.3%
10.4%	6.3%	0%	49.1%	8.3%	29.2%	8.3%	10.4%
0%	0%	6.9%	28.6%	6.9%	34.5%	13.8%	17.2%
2.8%	0%	0%	35.3%	5.6%	19.4%	22.2%	5.6%
3.3%	0%	0%	56.3%	16.7%	33.3%	13.3%	6.7%
1.4%	0%	5.7%	20.0%	4.3%	11.4%	8.6%	11.4%

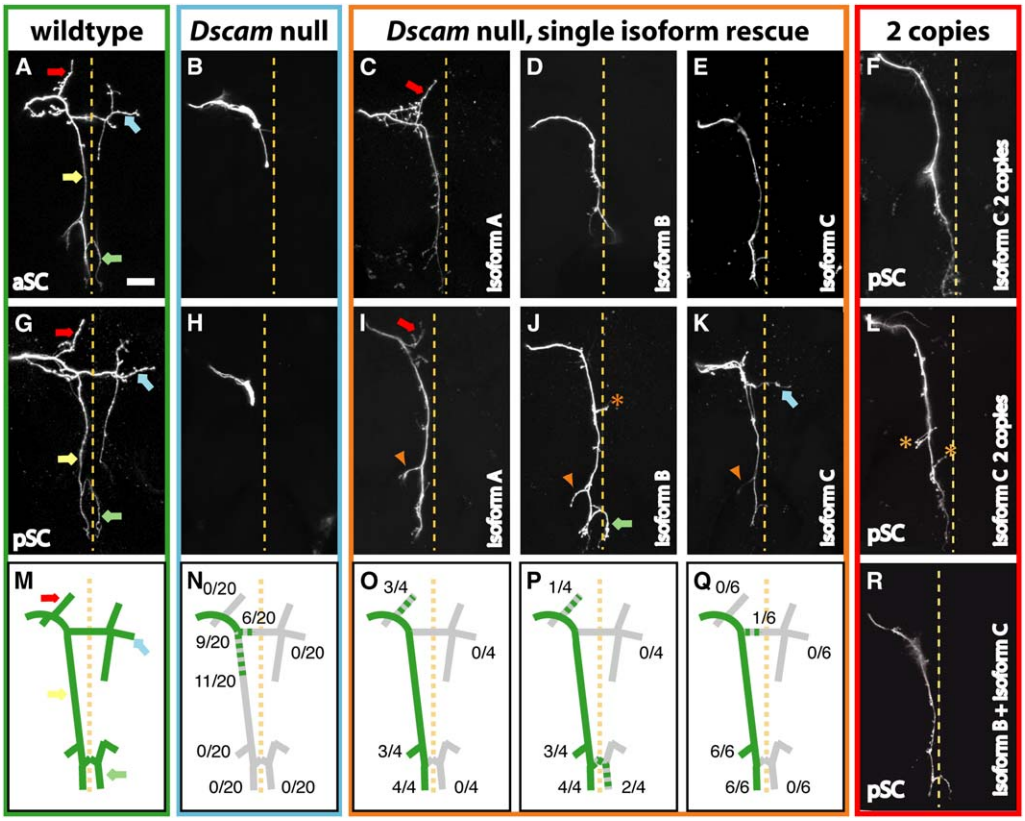

Figure 3. Single Dscam Isoforms Can Rescue the Basic Primary Axon Branch Extension but Not Specific Branch Targeting

(A and G) Wild-type branching patterns of aSc and pSc neurons in control animals. Scale bar = 50 μm.

(B and H) Axons that lack Dscam cannot extend normal branches and remain tightly clustered.

(C and I) Expression of a single Dscam isoform (A = 1.30.30.2) exclusively within Dscam null neurons only partially rescues the null phenotype. Occasionally isoform A rescued the proximal, anterior-extending secondary axonal branch (red arrow) and a distal ipsilateral branch (arrowhead).

(D and J) The single Dscam isoform B (1.34.30.2) equally rescues the primary axon extension posteriorly. Occasionally a distal ipsilateral branch (arrowhead) and a posterior midline-crossing branch (arrow) were present. However, no proximal anterior branch was observed. In contrast, an abnormal mesothoracic branch (asterisk) was observed in (J).

(E and K) Isoform C (7.6.19.2) also can restore the primary axon extension in Dscam null ms-neurons. The secondary branch structures that are specific to the aSc or pSc neurons, however, are generally not rescued. A single example of a contralateral extending branch was found (arrow).

(F, L, and R) Two copies of single Dscam isoforms within Dscam null neurons do not rescue the axonal branch phenotype. Ms-axons with two copies of Dscam isoforms enter the CNS correctly and exhibit normal posterior extension. However, these neurons occasionally overextend the primary branch beyond the metathoracic neuromere.

(M–Q) Schematic of the pSc axonal arbors from wild-type, Dscam null, and Dscam null plus single isoform ms-neurons. The observed frequencies of specific branch formations in pSc and aSc neurons are shown next to each branch (# observed / # samples total). Dotted lines mark the midline of the CNS. Abnormal ectopic branches are indicated by asterisks (L).

provide a suitable approach for a systematic analysis of Dscam isoform specificity. We therefore sought to test the functional importance of isoform diversity by only moderately reducing the Dscam diversity while maintaining the specific expression control of the endogenous Dscam gene. Fly strains were generated that selectively lack alternative exon 4 sequences due to small genomic deletions. This was accomplished using imprecise P-element excision of the *Dscam*^{P05518} allele, which carries a P-element located between exon 4.3 and 4.4 (Figure 4A and Experimental Procedures) (Schmucker et al., 2000). Two revertant fly lines were created where sequences spanning five alternative exon 4 sequences were removed (*Dscam*$^{\Delta R265}$ and *Dscam*$^{\Delta R272}$). The *Dscam*$^{\Delta R265}$ revertant strain lacks alternative exon 4 sequences 4.2–4.6, and the *Dscam*$^{\Delta R272}$ strain has a different subset of five exon 4 sequences deleted, 4.4–4.8 (Figure 4A). Both strains have a 41.7% reduction in exon 4 diversity and hence limit the maximally expressed number of potential isoforms to 22,176. We also generated two "clean-excision" strains, designated R43 and R87, which represent a complete reversion of the *Dscam*^{P05518} allele to wild-type, as confirmed by sequencing and phenotypic analysis (Experimental Procedures). *D*scam$^{\Delta R265}$, *D*scam$^{\Delta R272}$, R43, and R87 were generated from the same parental strain carrying the *Dscam*^{P05518} allele and thus share an identical

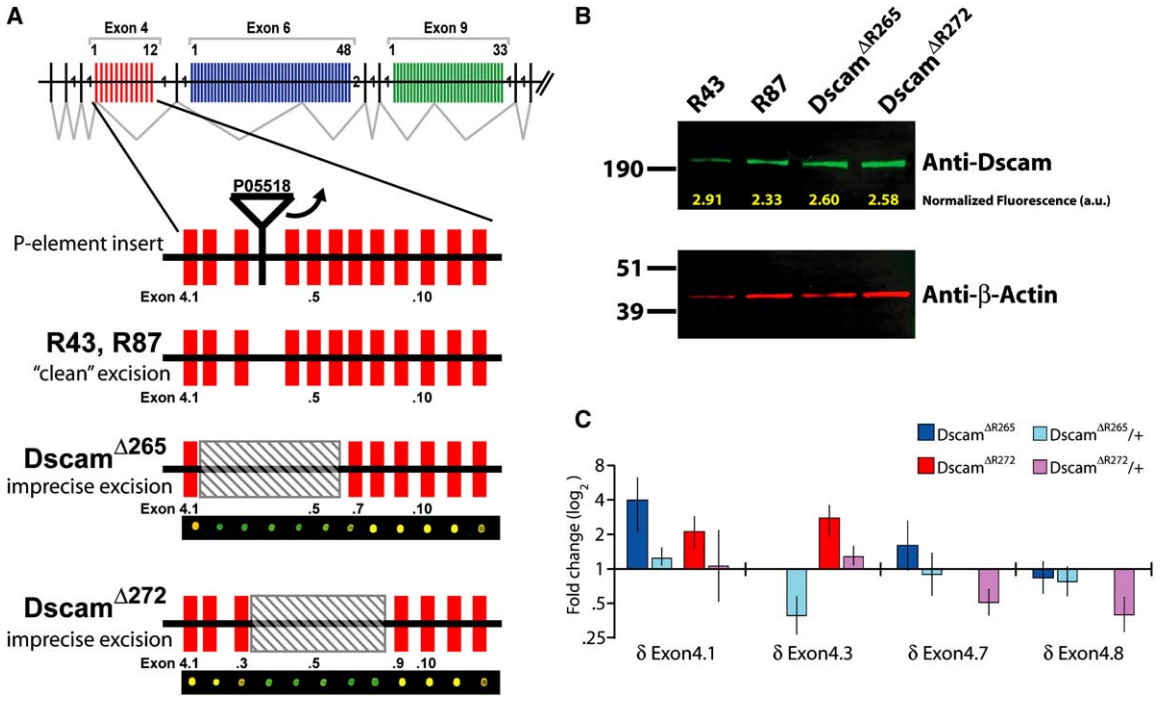

Figure 4. Molecular Analysis of Reduced Diversity Alleles

(A) Partial Dscam gene map and expanded view of exon 4 cluster indicating deficiency borders. The *Dscam*^{P05518} allele was mobilized to induce small deletions. Two "clean" excision strains were created, R43 and R87. *Dscam*$^{\Delta R265}$ flies lack alternative sequences 4.2–4.6, whereas *Dscam*$^{\Delta R272}$ flies lack sequences 4.4–4.8. Microarray analysis of *Dscam*$^{\Delta R265}$ and *Dscam*$^{\Delta R272}$ flies confirmed the deletion of excised sequences and intact expression of remaining sequences (examples with images of array spots are shown underneath each corresponding exon sequence; RNA levels from reduced diversity flies are in red; levels in control flies are green).

(B) Dscam protein levels in revertant flies are similar to clean-excision flies. Semiquantitative fluorescent Western blot analysis was used, and fluorescence levels (green) were normalized to β actin levels (red), which are listed in arbitrary units (a.u.) underneath each band.

(C) Some exon 4 sequences are upregulated in *Dscam*$^{\Delta R265}$ and *Dscam*$^{\Delta R272}$ flies. Quantitative real-time PCR analysis of the reduced diversity fly strains showed a 2- to 4-fold upregulation of the exon 4 sequences directly upstream of the excision. Heterozygous flies (*Dscam*$^{\Delta R265}$/+ and *Dscam*$^{\Delta R272}$/+) have up to 50% reduction in the exon 4 sequences that are excised in the parental revertant strains. Error bars are standard deviation from the mean.

genetic background. We therefore used flies with R43/R43, R87/R87, and R43/87 genotypes as wild-type control strains.

First, we examined whether deletion of genomic sequences in the exon 4 cluster could alter the overall Dscam protein expression. Semiquantitative Western blot analysis of Dscam protein showed no detectable difference in overall expression among the different fly strains (Figure 4B). The lack of any truncated forms of Dscam indicated that no exon skipping occurred in the revertant fly strains. Although it is difficult to detect small deviations of protein levels by western blot analysis, the potential changes in Dscam protein levels in *Dscam*$^{\Delta R265}$ or *Dscam*$^{\Delta R272}$ alleles are certainly significantly less than the expected 50% reduction in heterozygous *Dscam*^{LOF}/+ animals, which were used as controls in the phenotypic analysis described below.

The deletion of genomic sequences within the exon 4 cluster may influence the regulation of alternative splicing in *Dscam*$^{\Delta R265}$ or *Dscam*$^{\Delta R272}$ alleles. Custom-made oligo-arrays (Watson et al., 2005) were used to analyze the mRNA splice variant distribution in the larval CNS of different genotypes (Experimental Procedures). Comparative expression analysis of all of the 81 alternative exons 6 and 9 sequences revealed no significant differences between control and *D*scam$^{\Delta R265}$ or *D*scam$^{\Delta R272}$ flies (Experimental Procedures), consistent with studies showing independent and different splicing signals controlling alternative splicing of exon 4 and exon 6 clusters (Kreahling and Graveley, 2005). Analysis of the exon 4 sequences confirmed the absence of exons in *Dscam*$^{\Delta R265}$ or *Dscam*$^{\Delta R272}$ alleles and revealed a compensatory upregulation of the remaining alternative exon 4 sequences. Considering that the overall Dscam protein and mRNA levels in *D*scam$^{\Delta R265}$ and *D*scam$^{\Delta R272}$ CNS appear unaltered, one would expect a 1.7-fold increase in expression of remaining exon 4 sequences. However, the relative increase in expression of exon 4 sequences in *D*scam$^{\Delta R265}$ or *D*scam$^{\Delta R272}$ flies differed among the remaining exon 4 sequences. In particular, expression of exons 4.1 and 4.3, which are directly upstream of the deletions, are more strongly upregulated in the *D*scam$^{\Delta R265}$ or *D*scam$^{\Delta R272}$

alleles, respectively (Figure 4C). We confirmed the changes seen by microarray analysis using quantitative real-time PCR and found a 4-fold and 2-fold increase in exon 4.1 expressions in *Dscam*$^{\Delta R265}$ and *Dscam*$^{\Delta R272}$ flies, respectively. We also found a 3-fold increase in exon 4.3 expression in *Dscam*$^{\Delta R272}$ flies compared to control flies (Experimental Procedures). The quantitative measurements suggest that the deletion in exon 4 sequences resulted in a bias toward alternative exon sequences upstream of the deletion, whereas alternative exon sequences downstream of the deletions were slightly underrepresented.

These results show that alternative splicing is intact in *Dscam*$^{\Delta R265}$ or *Dscam*$^{\Delta R272}$ flies and that a considerable diversity of Dscam isoforms is still expressed in Dscam$^{\Delta R265}$ and Dscam$^{\Delta R272}$. However, the set of isoforms expressed in *Dscam*$^{\Delta R265}$ is not identical to the set expressed in *Dscam*$^{\Delta R272}$, and due to the exon 4 splicing bias in both mutant strains, some cells likely express different isoforms than wild-type cells. Overall, *Dscam*$^{\Delta R265}$ or *Dscam*$^{\Delta R272}$ likely express less of the isoform diversity than the predicted 22,176 possible alternative exon combinations.

Precision of Axonal Targeting Is Disrupted in *Dscam*$^{\Delta R265}$ and *Dscam*$^{\Delta R272}$ Mutant Flies

We examined the branching and connectivity of ms-neurons in *Dscam*$^{\Delta R265}$ and *Dscam*$^{\Delta R272}$ mutant flies and addressed two questions: First, is the precision of targeting quantitatively or qualitatively impaired in *Dscam*$^{\Delta R265}$ and *Dscam*$^{\Delta R272}$? Second, are there phenotypic differences between fly strains that have numerically equal but nonidentical repertoires of isoforms?

We found that 95% of *Dscam*$^{\Delta R265}$ and *Dscam*$^{\Delta R272}$ flies exhibited defects or deviations of pSc axon branching or extension when compared to the prototypic wild-type pattern (Figures 5 and 6) (Experimental Procedures). *Dscam*$^{\Delta R265}$ or *Dscam*$^{\Delta R272}$ flies had several phenotypes: mis-routing of axonal branches, formation of ectopic branches, lack of axonal branches, abnormal ipsilateral or contralateral projections, or early termination of axonal branches. Quantification of the phenotypic characterization is summarized in Table 1 and Table S1. We distinguished between phenotypic features that we never observed in wild-type animals (Group 1 = targeting errors) and deviations that we only rarely observed in controls (3%–16%) (Group 2 = variable targeting). Axonal branching defects that never occurred in wild-type flies (Group 1 errors) were observed in both *Dscam*$^{\Delta R265}$ and *Dscam*$^{\Delta R272}$ flies, indicating that the full diversity of exon 4 in these Dscam mutant flies is required for proper axonal targeting. Importantly, these defects were also observed in *trans*-allelic combinations of *Dscam*$^{\Delta R265}$/Dscam^{21}, *Dscam*$^{\Delta R265}$/Dscam$^{Df(2R)6055}$, *Dscam*$^{\Delta R272}$/Dscam^{21}, and *Dscam*$^{\Delta R272}$/Dscam$^{Df(2R)6055}$ (Figures 5 and 6 and Table 1). The severity of most classes of targeting defects (Group 1) observed in homozygous *Dscam*$^{\Delta R265}$ and *Dscam*$^{\Delta R272}$ flies was occasionally enhanced in *trans*-allelic combinations (Figure S3). This strongly suggests that these phenotypes are Dscam specific and not due to unrelated second site mutations.

The variability in neuronal connectivity (Group 2) was greatly enhanced in *Dscam*$^{\Delta R265}$ and *Dscam*$^{\Delta R272}$ flies. For example, the occurrence of an ectopic mesothoracic branch observed in 16% of wild-type flies increased to 70% in *Dscam*$^{\Delta R265}$ and to 49% in *Dscam*$^{\Delta R272}$ flies (Table 1). Furthermore, the percentage of flies that had multiple deviations in the pSc connectivity increased strongly. Only 8% of wild-type flies with more than one deviation from the prototypic pSc branching pattern was observed. In contrast, 39% of *Dscam*$^{\Delta R265}$ and 54% of *Dscam*$^{\Delta R272}$ flies had multiple axonal deviations, occasionally combined with one or more targeting errors (Table S2). It is important to note that whereas heterozygous *Dscam*$^{\Delta R265}$/+, *Dscam*$^{\Delta R272}$/+, or *Dscam*^{LOF}/+ flies showed few targeting defects (Group 1, Table 1), these flies do show a significant increase in variability of the connectivity pattern (Group 2, Tables 1 and S2). This enhancement of variability in heterozygous flies suggests a complex requirement for both Dscam diversity as well as Dscam expression levels. The variability in the axonal branching pattern seen in *Dscam*^{LOF}/+ indicates that an overall reduction of the Dscam expression level (heterozygosity) impairs the precision of axon branch connectivity. In contrast, *Dscam*$^{\Delta R265}$/+ or *Dscam*$^{\Delta R272}$/+ flies still have both copies of the Dscam gene, and the overall protein expression level is not changed. However, the variability in connectivity was higher in *Dscam*$^{\Delta R265}$/+ and *Dscam*$^{\Delta R272}$/+ than in *Dscam*^{LOF}/+. It is therefore possible that these are dominant effects due to a disproportionate increase of certain isoforms in ms-neurons. Alternatively, this increase in variability in heterozygous animals may reflect a requirement for expressing a specific combination of exon 4 alternates.

Phenotypic Differences in Flies Expressing Different Subsets of Isoforms

Analysis of the frequency distribution of targeting or branching errors showed a significant difference between *Dscam*$^{\Delta R265}$ and *Dscam*$^{\Delta R272}$ flies ($p < 0.001$), and the axonal branching patterns were qualitatively distinct (Figures 5 and 6). For example, in *Dscam*$^{\Delta R265}$ flies, ectopic branches within the prothoracic region of the CNS occurred at a 20% frequency (n = 66; Ectopic branch "1" in Figure 5N). This ectopic branch rarely occurred in *Dscam*$^{\Delta R272}$ flies (5%; n = 56) and was never seen in wild-type flies (n = 81) (Table 1). A different ectopic branch in the mesothoracic region of the CNS (Ectopic branch "2" in Figure 5N) was observed most frequently in *Dscam*$^{\Delta R265}$ flies (70%) and often crossed the midline (arrow in Figures 5G and 5H). This branch occurred less frequently in *Dscam*$^{\Delta R272}$ flies (~50%; $p < 0.005$) and in 16% of control animals (Table 1). It is important to note that this mesothoracic ectopic branch in *Dscam*$^{\Delta R265}$ pSc neurons always occurred at the same location (Figure S4). This location coincides precisely with a presumptive "decision point" where axons of pDc neurons normally extend a branch to

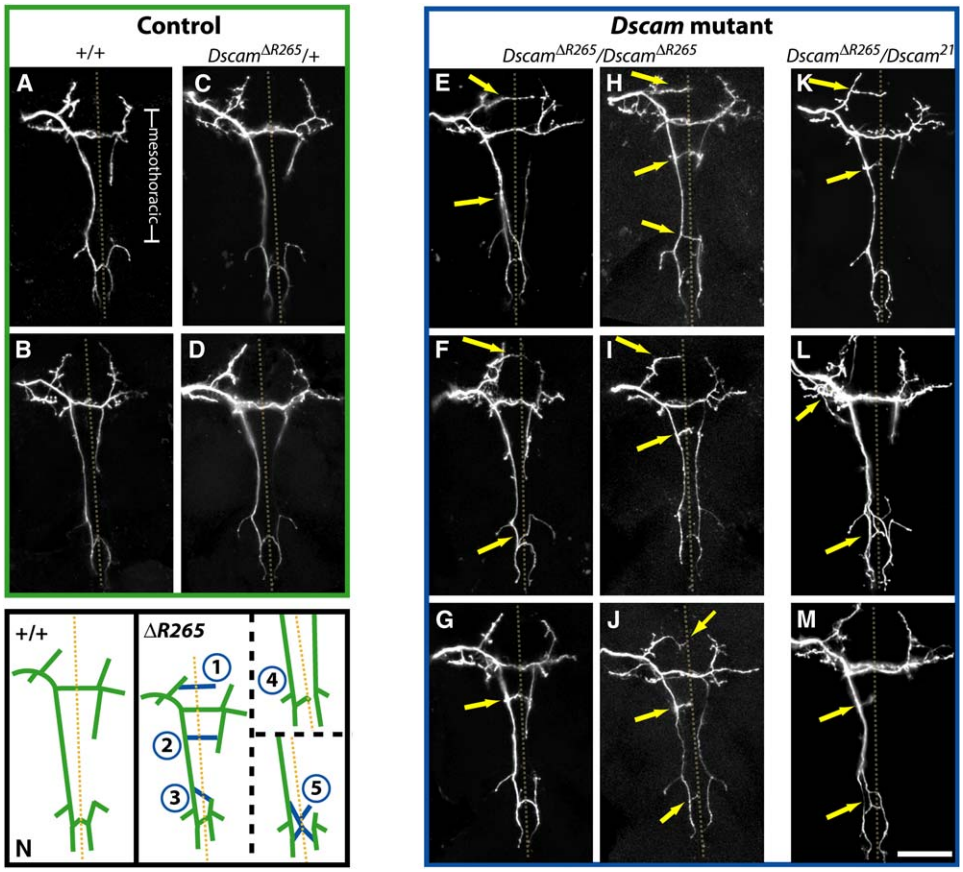

Figure 5. *Dscam*$^{\Delta R265}$ Flies Exhibit Characteristic Connectivity Errors

(A–D) The pSc branching pattern in control animals. The pSc neuron in "clean-excision" flies, R43 or R87, is labeled with fluorescent dye (A and B). The axonal arbor within the mesothoracic neuromere is shown in (A). Dotted lines mark the midline of the CNS. The pSc neuron of heterozygous flies, *Dscam*$^{\Delta R265}$/R43 or *Dscam*$^{\Delta R265}$/R87, has a wild-type branching pattern (C and D).

(E–M) Dscam mutant flies lacking 42% isoform diversity have multiple axon targeting errors and deviations from the prototypic wild-type projection pattern. *Dscam*$^{\Delta R265}$ homozygous mutant flies have ectopic branch errors in the pro- and mesothoracic neuromeres. *Dscam*$^{\Delta R265}$ transheterozygous flies with a Dscam null allele (*Dscam*^{21}) have similar but slightly more severe defects compared to *Dscam*$^{\Delta R265}$ homozygotes. *Dscam*$^{\Delta R265}$ /*Dscam*^{21} flies have multiple ectopic axonal branches (arrows). Errors are denoted by arrows. Scale bar = 50 μm.

(N) Schematic depicting errors common to *Dscam*$^{\Delta R265}$ mutant flies. The left panel depicts branching of primary and secondary axonal branches in control flies. The right panel depicts a summary of errors that occur with a frequency of 13%–70% (see text) in *Dscam*$^{\Delta R265}$ mutant flies.

contralateral targets. This supports a role of Dscam in specifying appropriate or suppressing inappropriate axon branch extension rather than simply a control of axon branch segregation.

Phenotypes of *Dscam*$^{\Delta R272}$ flies were qualitatively more severe (Figure 6). More than half of *Dscam*$^{\Delta R272}$ flies had multiple errors along the pSc axon, and the distribution of targeting errors was broader. For example, the main primary axon extension (Figures 3C–3F, 3I–3L, and 3R) misrouted across the midline contralaterally in 13% of *Dscam*$^{\Delta R272}$ flies and also included ectopic branches along the posterior midline (arrow in Figure 6I). The main primary extension occasionally failed to branch contralaterally (10%) or extended directly along the midline typically with several small ectopic branches (10%) or was completely truncated and failed to innervate the metathoracic region (6%) (Figure 6J).

Flies with trans-allelic combinations of *Dscam*$^{\Delta R265}$/*Dscam*$^{\Delta R272}$ lack both copies of exon sequences 4.4, 4.5, and 4.6 and have one remaining copy of the exon sequences 4.2, 4.3, 4.7, and 4.8. This reduces the maximal number of possible Dscam isoforms by 25%. Although 86% of *Dscam*$^{\Delta R265}$/*Dscam*$^{\Delta R272}$ flies had pSc defects or deviations from the prototypic axonal branching pattern, the penetrance of Group 1 targeting errors was lower (~20%) (Table 1). Nevertheless, 46% of the ms-neurons exhibited multiple targeting defects or deviations along a single axonal projection. Importantly, we observed a reduction in phenotypic defects that are characteristic of either *Dscam*$^{\Delta R265}$ or *Dscam*$^{\Delta R272}$ homozygous flies (Figure S3).

Our analysis of the pSc targeting errors in *Dscam*$^{\Delta R265}$ and *Dscam*$^{\Delta R272}$ flies demonstrates a requirement for Dscam diversity in precise axonal targeting. The allele-specific differences between *Dscam*$^{\Delta R265}$ and *Dscam*$^{\Delta R272}$

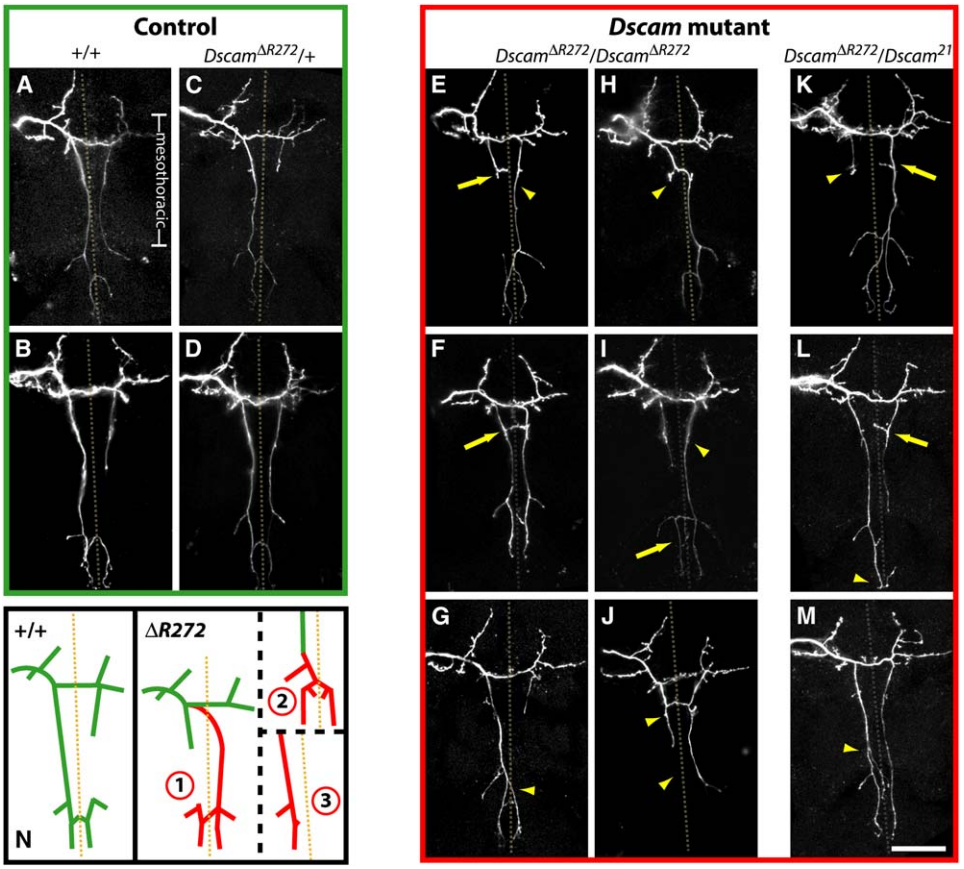

Figure 6. *Dscam*$^{\Delta R272}$ Flies Exhibit Axonal Targeting Errors

(A–D) The axon branching pattern in control animals. The pSc neuron in control flies, or transheterozygous flies, *Dscam*$^{\Delta R272}$/R43 or *Dscam*$^{\Delta R272}$/R87 has few deviations from the prototypic wild-type branching pattern.

(E–J) *Dscam*$^{\Delta R272}$ mutant flies exhibit axonal connectivity errors predominantly toward the posterior CNS region. *Dscam*$^{\Delta R272}$ flies have more severe axon branch "routing" errors (arrowheads) rather than the stereotyped ectopic branch errors in *Dscam*$^{\Delta R265}$ (Figure 5). The main primary axon extension that occurs ipsilaterally in wild-type flies often extends contralaterally (E, H, and I) or completely fails to extend posteriorly (J).

(K–M) The pSc neurons of *Dscam*$^{\Delta R272}$/*Dscam*^{LOF} flies have defects similar to *Dscam*$^{\Delta R272}$ homozygotes. Multiple errors of axonal misrouting (arrowheads) and ectopic branches (arrows) were common among *Dscam*$^{\Delta R272}$ flies. Scale bar = 50 μm.

(N) Schematic of axonal branch errors common to *Dscam*$^{\Delta R272}$ mutant flies. Left panel: control flies. The right panel depicts errors that occur with a frequency of 10%–30% (see text) in *Dscam*$^{\Delta R272}$ mutant flies.

flies suggest that alternative exon 4 sequences have non-redundant functions during axonal targeting.

DISCUSSION

Alternative splicing at the *Drosophila* Dscam locus potentially generates 38,016 receptor isoforms, which are expressed in the nervous system and the immune system of flies (Schmucker et al., 2000; Watson et al., 2005). Genetic studies have shown that Dscam is an essential gene and functionally required in both systems (Schmucker et al., 2000; Wang et al., 2002; Hummel et al., 2003; Watson et al., 2005). However, it has been technically challenging to obtain evidence that the large diversity of Dscam isoforms is utilized for generating specificity during neuronal wiring or immune recognition. Here we have described a genetic analysis of Dscam function in the somatosensory system of flies and provide evidence that the precision of neuronal connectivity of sensory neurons depends on a large isoform diversity.

Dscam Is Essential for Multiple Aspects of Axonal Targeting

Lack of Dscam results in a fully penetrant and striking phenotype in which axonal branches are entangled at a presumptive decision point within the CNS. Because Dscam null ms-axons could pathfind into the CNS correctly, this phenotype suggests that these axons normally undergo a transition from a "guidance-mode" to a "targeting-mode" once a decision point within the CNS is reached. Our genetic analysis shows that Dscam is not required during the guidance-mode but is essential for controlling multiple aspects of ms-neuron targeting.

Different Dscam isoforms were each capable of significantly rescuing the posterior oriented primary axon extension but failed to appreciably rescue subsequent targeting steps. Previous studies addressing the functional differences of receptor isoforms have demonstrated the importance of protein levels in assessing potential phenotypic rescues (Nern et al., 2005). It has been shown that in some developmental context expression levels of receptor isoforms rather than potential differences in biochemical properties might be functionally important. However, this possibility seems unlikely to apply here: Increasing the Dscam protein level in rescue experiments did not provide any improvement of ms-neuron targeting. In addition, a potentially gradual decline of rescuing ability would be predicted for the distal versus proximal axonal segments if the amount of single Dscam isoform protein produced within ms-neurons were below a critical threshold. Although we found that isoform A exhibited some rescuing ability of the more proximal anterior branch (Figures 3C and 3I), isoform B did not rescue the anterior or contralateral branch but instead could occasionally rescue the most distal posterior branch (Figure 3J), which is inconsistent with a simple concentration-limited model.

We propose that Dscam has several functions during ms-neuron targeting. One function, which could be considered a "core" function, is to promote axon extension where many or all isoforms are likely to function equally well. In contrast, processes such as directional branch extension, branch stabilization, or formation of synaptic contacts could require a separate, potentially isoform-specific Dscam function. Considering the extraordinary diversity of Dscam, we posit that the core function of Dscam depends on a receptor-ligand interaction that may not engage the variable Ig-domains, whereas the differential signaling underlying specific targeting decisions involves isoform specific Ig-domains, possibly through homophilic interactions.

Are Alternative Exon 4 Sequences Redundant?

An analysis of Dscam function during mushroom body development revealed that deletion of exon 4 sequences had no obvious phenotypic consequences for axon bifurcation or general mushroom body development (Wang et al., 2004). This raised the possibility that alternative exon 4 sequences might be functionally redundant during axonal morphogenesis (Wang et al., 2004). In addition, expression studies suggested that many different isoforms are expressed in single mushroom body neurons, and alternative splicing of exon 4 and exon 6 appeared largely random. Functionally, it was shown that an almost complete phenotypic rescue of single mushroom body neurons could be achieved equally well with very different single isoforms (Zhan et al., 2004).

These results could be interpreted as evidence against the specificity of individual Dscam isoforms and as an indication that the large diversity of Dscam may not be functionally important. In addition, it is conceivable that the specificity of Dscam is mainly required for immune functions and not at all during neuronal differentiation (Watson et al., 2005). However, our analysis of the axonal targeting in the somatosensory system of flies provides evidence against redundancy of alternative exon 4 sequences and supports a specific role for exon 4 sequences in regulating targeting of individual axonal branches.

What is the basis for these seemingly conflicting findings? Although Dscam has multiple functions and a widespread requirement throughout nervous system development, it is likely that only some differentiation processes require diverse isoforms (Zhan et al., 2004). Therefore, a critical difference lies in the choice of experimental system used to assess isoform-specific functions of Dscam. First, studies on axon morphogenesis of mushroom body neurons have focused on a neuronal differentiation process that, even in the complete absence of any Dscam protein, occurs normally in more than half of the neurons examined (Wang et al., 2004; Zhan et al., 2004). Second, segregation of axons after bifurcation requires a simple binary decision of sister branches, and it has been proposed that interactions between identical isoforms of Dscam expressed on sister branches of the same mushroom body neurons produce a signal leading to repulsion (Wang et al., 2004; Zhan et al., 2004). Implicit to this model is the notion that any isoform, as long as it is the same on sister branches, can fulfill this repellent function. In contrast, the contribution of Dscam to neuronal connectivity in the somatosensory system is likely to be fundamentally different. Our analysis revealed that Dscam is essential for targeting of ms-neurons, and apparently no redundant receptor system could compensate for a lack of Dscam in ms-neurons. Furthermore, single ms-neurons and their multiple axonal branches have to make a series of independent and complex targeting decisions, which almost certainly will involve trans-interactions with membrane surfaces from cells expressing different Dscam isoforms. For example, the phenotypic differences of ms-neuron targeting in $Dscam^{\Delta R265}$ or $Dscam^{\Delta R272}$ flies (Figures 5 and 6) raise the intriguing possibility that targeting of ms-neurons involves restricted subcellular localization of different isoforms. We therefore propose that the inherent complexity underlying the molecular control of targeting decisions in ms-neurons depends on novel Dscam functions, which are different from functions of Dscam within mushroom body neurons.

Evidence That the Diversity of Dscam Proteins Produced by Alternative Splicing Is Functionally Important

Many aspects of *Drosophila* ms-neuron targeting are genetically hardwired, such as the position of primary or secondary axon branches, direction of branch extension, length of branch extension, and midline crossing. Our data suggest that Dscam receptor diversity plays a key role in the genetic control of precise neuronal wiring. We show that reducing the Dscam diversity by deleting exon 4 sequences produced errors of axonal branch extension and strongly increased variability in the axonal branching pattern (Figures 5 and 6). These defects were also observed

in *trans*-allelic combinations with Dscam loss-of-function alleles, suggesting that they are unlikely caused by unspecific or pleiotropic defects. Importantly, the genetic manipulations necessary to generate the $Dscam^{\Delta R265}$ and $Dscam^{\Delta R272}$ alleles did not compromise the overall Dscam protein level. Although quantitative analysis of alternative splicing showed a biased exon choice of the remaining exon 4 sequences, the only likely consequence of this bias in $Dscam^{\Delta R265}$ or $Dscam^{\Delta R272}$ cells is that not all exon 4, 6, 9, and 17 combinations are utilized at the same frequency as in wild-type. Nevertheless, expression analysis of $Dscam^{\Delta R265}$ and $Dscam^{\Delta R272}$ flies indicates that many thousands of diverse Dscam isoforms are expressed.

Although changes in position or number of small axonal branches within the CNS may be considered subtle defects, it is important to note that the properties of the *Drosophila* neuronal circuit depend critically on high precision, starting with the input from ms-neurons. For example, ms-neurons of different identities form unique branching patterns, where distinct axonal branches relay information through different synaptic connections with different target areas (Ghysen, 1980; Canal et al., 1998; Williams and Shepherd, 2002). The farther apart ms-neurons are, the more disparate are the corresponding branching patterns. This depends in part on the somatotopic order of peripheral ms-neuron projections and thereby is a reflection of the ability to decode important spatial sensory information (e.g., direction of airflow). In addition, some ms-neurons have been shown to control different reflexes, such as leg movement or a complex sequence of cleaning behaviors (Canal et al., 1998). Considering these circuit specializations, it seems imperative to ensure that the precision of the targeting of individual axonal branches of ms-neurons is under tight genetic control.

How Is Dscam Diversity Utilized during Axonal Targeting of ms-neurons?

Little is known about how specific axon branches and their extensions within the CNS are specified (Zlatic et al., 2003). For the pSc neuron, it has been shown that certain aspects of its axonal branching pattern depend on preexisting pioneer fibers (see Figures 4B–4D in Williams and Shepherd, 2002). Interestingly, ablation of these pioneer fibers produced phenotypic defects that are highly similar to the errors found in $Dscam^{\Delta R265}$ or $Dscam^{\Delta R272}$ flies. Specifically, flies that lacked one subset of pioneer fibers had pSc branching errors similar to those observed in $Dscam^{\Delta R265}$ (Figure 5). In contrast, animals lacking a second subset of pioneer fibers had branching defects resembling those in $Dscam^{\Delta R272}$ flies (Figure 6). Local interactions mediated by Dscam isoforms present on axons of ms-neurons as well as on axons of preexisting larval sensory neurons may therefore be important for branching and targeting decisions. We hypothesize that the precise and unique axonal branching patterns of the ms-neurons depend on a nonrandom combination and tightly controlled expression of specific Dscam isoforms in ms-neurons and target fibers within the CNS. Specifically, interactions of identical or highly similar isoforms could ensure suppression (i.e., repulsion) of ectopic branches. Such a model would be consistent with the high specificity of homophilic isoform interactions demonstrated in vitro and with the proposed model in which homophilic Dscam interactions trigger repulsion (Wojtowicz et al., 2004). Considering that the observed phenotypic connectivity errors or deviations occur only with partial penetrance (Table 1), we suggest that in vivo isoforms with the most similar Ig-2 domains interact with affinities sufficient to potentially compensate for each other, albeit at reduced efficiency.

Conclusion

Our genetic data on the importance of diverse exon 4 sequences are consistent with the provocative possibility that interactions between ms-neurons and pioneer fibers utilize different subsets of Dscam isoforms. In this model, specific receptor isoforms play an instructive role in the targeting of axonal branches. Considering the biochemical properties of Dscam isoforms (Wojtowicz et al., 2004), it seems intuitive to suggest that homophilic interactions may provide the molecular principle for this model. However, this hypothesis poses a series of profound molecular problems. What are the mechanisms controlling the proposed matching isoform expression or localization such that homophilic interactions can be utilized instructively? How strict is the isoform specificity or requirement of homophilic Dscam interactions in vivo? How are different Dscam isoforms localized to different axonal branches, branch points, different CNS fibers, or domains? Whatever the answers to these pressing questions may be, our analysis shows that dissecting the mechanisms by which Dscam controls neuronal wiring promises important contributions to a general understanding of the genetic control of wiring specificity.

EXPERIMENTAL PROCEDURES

MARCM Fly Generation

Flies of the following genotype were used: *hs*Flp, *elav-GAL4, UAS-CD8-GFP; FRT42D, Tubulin-GAL80* and *FRT42D,* $Dscam^{LOF}$*/CyO*. $Dscam^{LOF}$ alleles were previously described (Zhan et al., 2004; Zhu et al., 2006). Two heat shocks (37°C) were performed twice for 1 hr each, during early 3rd instar larval stage (~90 hr after egg laying). Anesthetized adult flies were screened for single GFP-positive ms-neurons using a Zeiss stereomicroscope under epifluorescence illumination.

Single Isoform Rescues

Total RNA was isolated from third instar larval brain using TRIzol (Invitrogen, Carlsbad, CA), and reverse transcription was performed on 30 ng of RNA using random primers (Invitrogen). To generate Dscam cDNA, including variable exons 4, 6, and 9, PCR amplification was performed using Pfu Turbo polymerase (Stratagene, LaJolla, CA). Five Dscam isoforms with different combinations of exon 4, 6, and 9 were isolated, and isoforms B (encoding alternative exons 4.1, 6.34, 9.30) and C (encoding 4.7, 6.6, 9.19) were selected for transgene construction and inserted in the P element expression vector (pUAST). Transgenic flies were generated as previously described (Watson et al., 2005).

Generating Reduced Diversity Alleles

P-element stock *Dscam*^{P05518}/CyO; ry/ry and *wg*^{Sp}/*CyO; Sb, Δ2-3/TM3, ry* were used to mobilize the P-element, and Southern and PCR analyses were performed on genomic DNA. Deletions and clean excisions were confirmed by sequencing: *Dscam*^{ΔR265} flies have the genomic sequence deleted starting from position (*Drosophila* genome sequence release AF260530.1) 15,522 (the intronic region 3′ of exon 4.1) to position 17,453 (20 base pairs into the 5′ intronic region of exon 4.7); *Dscam*^{ΔR272} flies have genomic sequences deleted from 16,513 (the intronic region 3′ of exon 4.3) to 17,952 (the middle of exon 4.8) and retain a 33 base pair 5′ footprint of the P-element. Dscam mRNA of revertant flies was independently analyzed using microarray and real-time PCR to confirm the absence of alternative exons.

Carbocyanine Dye Labeling

Labeling was done essentially as previously described (Grillenzoni et al., 1998). The dyes DiI, DiD, or DiO (Molecular Probes, Eugene, OR) were used at 0.3 mg/mL ethanol, and dye transfer was allowed to proceed for 2 days.

Confocal Microscopy and Image Analysis

Laser-scanning confocal microscopy was achieved using a Zeiss LSM 410 inverted confocal microscope using Kr/Ar laser for 488 nm and 568 nm excitation and He/Ne lasers for 543 nm and 633 nm excitation. Small *z*-stacks (~35 total, 1 μm spacing) were collected, and maximal *z*-projections were analyzed. The CNS width was measured to determine the variation in fly size, tissue fixation, or imaging angle. A generic branching skeleton was used as a standard from which to compare all pSc branching patterns (for details, see Supplemental Data). We found no significant differences between the lengths or positions (except for the position of Branch 10; see Supplemental Data) of the axonal branches between the Dscam mutant flies and wild-type flies (t test, $p > 0.05$), most likely due to the larger variance in phenotypes of mutant flies. A goodness-of-fit test based on the chi-square distribution was used to calculate statistical significance between *Dscam*^{ΔR265} and *Dscam*^{ΔR272} axonal phenotype distributions, and it was used in comparisons of single error categories (when the number of observations was greater than five) to determine statistical significance ($p < 0.05$). Images were analyzed using custom-written software in MatLab (Mathworks, Natick, MA).

Microarray Analysis

Microarray experiments were carried out as previously described (Watson et al., 2005). For sample preparation, R43, R87, *Dscam*^{ΔR265}, and *Dscam*^{ΔR272} genotypes were used. Third-instar larval brains were dissected, and total RNA was extracted using TRIzol (Invitrogen). PCR products were labeled by incorporation of Cy3-dUTP or Cy5-dUTP using the Bioprime labeling kit (Invitrogen) as described in Watson et al., 2005. Primer sequences are given in Supplemental Data. Dye swap experiments were performed for each of the RNA samples to control for potential dye incorporation biases.

Signal and background fluorescence for each array spot were obtained using the GenePix Pro 5.1 software. Labeled DNA samples were obtained from two separate PCR reactions (exons 3–7 and exons 8–11); therefore, constant exons 5 and 7 were used to normalize variable exons 4 and 6 signals, and constant exons 10 and 11 were used to normalize signals for variable exon 9. Using these constant exons, fluorescent signals were normalized to obtain a 532 nm (Cy3) / 635 nm (Cy5) mean ratio of 1 for background subtracted signals. Further analysis was done using custom written software in MatLab, available on request (Mathworks). Negative control spots were then subtracted to correct for mishybridizations. Expression level changes in exon sequences were from two to six experiments for each sample (with each experiment represented by the mean of the triplicate value). Statistical significance of expression levels between different exon sequences was determined using t test with Bonferroni correction to control the overall Type I error to 5%.

Quantitative Real-Time PCR Analysis

Total RNA of third-instar (wandering) larval brains was isolated as described in Watson et al., 2005. Reverse transcription was performed using random hexamers as primers (Invitrogen). Real-time PCR was performed on ~10 ng of cDNA product in a total volume of 25 μL using TaqMan PCR Mix (Applied Biosystems, Foster City, CA). Samples in each experiment were performed in duplicate or quadruplicate. PCR amplification was detected using an AB7300 Real Time PCR System (Applied Biosystems), and cycle threshold (CT) was determined using the AB7300 System SDS software. Threshold was defined as the fluorescence intensity significantly above background during the exponential phase of PCR amplification for all reactions. The cycle number at which each sample crossed the threshold was recorded. CT values were normalized to *Rp49* control levels and averaged within each experiment. Mean CT values and standard deviations of the mean of three to ten experiments were used for each sample.

Dscam Protein Analysis

Third-instar larval brains were dissected, and total protein was extracted in RIPA buffer with protease inhibitor (Roche, Indianapolis, IN). Samples were run on a 4%–12% Bis-Tris polyacylamide gel (Invitrogen) and transferred onto PVDF membranes. Membranes were incubated with primary antibodies (D-cy) to Dscam (Watson et al., 2005) and β actin (Sigma-Aldrich), and secondary antibodies were conjugated to infrared dyes (Rockland Immunochemicals, Gilbertsville, PA). Semiquantitative detection of protein levels was performed using the LiCor Odyssey Infrared Imager (Lincoln, NE). Integrated fluorescence intensities of individual bands were measured and background subtracted using the Odyssey Application software. Dscam bands were normalized to β actin, and results from six experiments were used for analysis (t test, $p > 0.05$).

Supplemental Data

Supplemental Data include four figures, two tables, Experimental Procedures, and References and can be found with this article online at http://www.cell.com/cgi/content/full/125/3/607/DC1/.

ACKNOWLEDGMENTS

We thank B. Sabatini, Q. Ma, and members of the Schmucker lab for critical reading of the manuscript. We thank the Bloomington *Drosophila* Stock Center and the labs of L. Luo and L. Zipursky for fly stocks. This research was supported by the NIH (RO1-NS46747) (D.S.); a Pew Scholars Program Award (D.S.); a John Merck Fund Award (D.S.); a postdoctoral fellowship from training grant T32CA09361 DFCI (B.E.C.); and an Edward R. and Anne G. Lefler Center postdoctoral fellowship (M.K.).

Received: February 20, 2006
Revised: March 19, 2006
Accepted: March 29, 2006
Published: May 4, 2006

REFERENCES

Ango, F., di Cristo, G., Higashiyama, H., Bennett, V., Wu, P., and Huang, Z.J. (2004). Ankyrin-based subcellular gradient of neurofascin, an immunoglobulin family protein, directs GABAergic innervation at purkinje axon initial segment. Cell *119*, 257–272.

Benson, D.L., Colman, D.R., and Huntley, G.W. (2001). Molecules, maps and synapse specificity. Nat. Rev. Neurosci. *2*, 899–909.

Boucard, A.A., Chubykin, A.A., Comoletti, D., Taylor, P., and Sudhof, T.C. (2005). A splice code for trans-synaptic cell adhesion mediated by binding of neuroligin 1 to alpha- and beta-neurexins. Neuron *48*, 229–236.

Boulanger, L.M., and Shatz, C.J. (2004). Immune signalling in neural development, synaptic plasticity and disease. Nat. Rev. Neurosci. *5*, 521–531.

Canal, I., Acebes, A., and Ferrus, A. (1998). Single neuron mosaics of the *Drosophila* gigas mutant project beyond normal targets and modify behavior. J. Neurosci. *18*, 999–1008.

Cheng, H.J., Nakamoto, M., Bergemann, A.D., and Flanagan, J.G. (1995). Complementary gradients in expression and binding of ELF-1 and Mek4 in development of the topographic retinotectal projection map. Cell *82*, 371–381.

Feinstein, P., and Mombaerts, P. (2004). A contextual model for axonal sorting into glomeruli in the mouse olfactory system. Cell *117*, 817–831.

Flanagan, J.G., and Vanderhaeghen, P. (1998). The ephrins and Eph receptors in neural development. Annu. Rev. Neurosci. *21*, 309–345.

Ghysen, A. (1978). Sensory neurones recognise defined pathways in Drosophila central nervous system. Nature *274*, 864–872.

Ghysen, A. (1980). The projection of sensory neurons in the central nervous system of Drosophila: choice of the appropriate pathway. Dev. Biol. *78*, 521–541.

Grillenzoni, N., van Helden, J., Dambly-Chaudiere, C., and Ghysen, A. (1998). The iroquois complex controls the somatotopy of *Drosophila* notum mechanosensory projections. Development *125*, 3563–3569.

Hindges, R., McLaughlin, T., Genoud, N., Henkemeyer, M., and O'Leary, D.D. (2002). EphB forward signaling controls directional branch extension and arborization required for dorsal-ventral retinotopic mapping. Neuron *35*, 475–487.

Huber, A.B., Kolodkin, A.L., Ginty, D.D., and Cloutier, J.F. (2003). Signaling at the growth cone: ligand-receptor complexes and the control of axon growth and guidance. Annu. Rev. Neurosci. *26*, 509–563.

Huh, G.S., Boulanger, L.M., Du, H., Riquelme, P.A., Brotz, T.M., and Shatz, C.J. (2000). Functional requirement for class I MHC in CNS development and plasticity. Science *290*, 2155–2159.

Hummel, T., Vasconcelos, M.L., Clemens, J.C., Fishilevich, Y., Vosshall, L.B., and Zipursky, S.L. (2003). Axonal targeting of olfactory receptor neurons in *Drosophila* is controlled by Dscam. Neuron *37*, 221–231.

Kohmura, N., Senzaki, K., Hamada, S., Kai, N., Yasuda, R., Watanabe, M., Ishii, H., Yasuda, M., Mishina, M., and Yagi, T. (1998). Diversity revealed by a novel family of cadherins expressed in neurons at a synaptic complex. Neuron *20*, 1137–1151.

Kreahling, J.M., and Graveley, B.R. (2005). The iStem, a long-range RNA secondary structure element required for efficient exon inclusion in the *Drosophila* Dscam pre-mRNA. Mol. Cell. Biol. *25*, 10251–10260.

Lee, T., and Luo, L. (1999). Mosaic analysis with a repressible cell marker for studies of gene function in neuronal morphogenesis. Neuron *22*, 451–461.

Missler, M., Hammer, R.E., and Sudhof, T.C. (1998). Neurexophilin binding to alpha-neurexins. A single LNS domain functions as an independently folding ligand-binding unit. J. Biol. Chem. *273*, 34716–34723.

Nern, A., Nguyen, L.V., Herman, T., Prakash, S., Clandinin, T.R., and Zipursky, S.L. (2005). An isoform-specific allele of *Drosophila* N-cadherin disrupts a late step of R7 targeting. Proc. Natl. Acad. Sci. USA *102*, 12944–12949.

Neves, G., Zucker, J., Daly, M., and Chess, A. (2004). Stochastic yet biased expression of multiple Dscam splice variants by individual cells. Nat. Genet. *36*, 240–246.

Schmucker, D., Clemens, J.C., Shu, H., Worby, C.A., Xiao, J., Muda, M., Dixon, J.E., and Zipursky, S.L. (2000). *Drosophila* Dscam is an axon guidance receptor exhibiting extraordinary molecular diversity. Cell *101*, 671–684.

Sperry, R.W. (1963). Chemoaffinity in the Orderly Growth of Nerve Fiber Patterns and Connections. Proc. Natl. Acad. Sci. USA *50*, 703–710.

Takeichi, M., Matsunami, H., Inoue, T., Kimura, Y., Suzuki, S., and Tanaka, T. (1997). Roles of cadherins in patterning of the developing brain. Dev. Neurosci. *19*, 86–87.

Tessier-Lavigne, M., and Goodman, C.S. (1996). The molecular biology of axon guidance. Science *274*, 1123–1133.

Uemura, T. (1998). The cadherin superfamily at the synapse: more members, more missions. Cell *93*, 1095–1098.

Vassalli, A., Rothman, A., Feinstein, P., Zapotocky, M., and Mombaerts, P. (2002). Minigenes impart odorant receptor-specific axon guidance in the olfactory bulb. Neuron *35*, 681–696.

Wang, F., Nemes, A., Mendelsohn, M., and Axel, R. (1998). Odorant receptors govern the formation of a precise topographic map. Cell *93*, 47–60.

Wang, J., Zugates, C.T., Liang, I.H., Lee, C.H., and Lee, T. (2002). *Drosophila* Dscam is required for divergent segregation of sister branches and suppresses ectopic bifurcation of axons. Neuron *33*, 559–571.

Wang, J., Ma, X., Yang, J.S., Zheng, X., Zugates, C.T., Lee, C.H., and Lee, T. (2004). Transmembrane/juxtamembrane domain-dependent Dscam distribution and function during mushroom body neuronal morphogenesis. Neuron *43*, 663–672.

Watson, F.L., Püttmann-Holgado, R., Thomas, F., Lamar, D.L., Hughes, M., Kondo, M., Rebel, V.I., and Schmucker, D. (2005). Extensive diversity of Ig-superfamily proteins in the immune system of insects. Science *309*, 1874–1878.

Weiner, J.A., Wang, X., Tapia, J.C., and Sanes, J.R. (2005). Gamma protocadherins are required for synaptic development in the spinal cord. Proc. Natl. Acad. Sci. USA *102*, 8–14.

Williams, D.W., and Shepherd, D. (2002). Persistent larval sensory neurones are required for the normal development of the adult sensory afferent projections in Drosophila. Development *129*, 617–624.

Wojtowicz, W.M., Flanagan, J.J., Millard, S.S., Zipursky, S.L., and Clemens, J.C. (2004). Alternative splicing of *Drosophila* Dscam generates axon guidance receptors that exhibit isoform-specific homophilic binding. Cell *118*, 619–633.

Wu, Q., and Maniatis, T. (1999). A striking organization of a large family of human neural cadherin-like cell adhesion genes. Cell *97*, 779–790.

Yamagata, M., Weiner, J.A., and Sanes, J.R. (2002). Sidekicks: synaptic adhesion molecules that promote lamina-specific connectivity in the retina. Cell *110*, 649–660.

Zhan, X.L., Clemens, J.C., Neves, G., Hattori, D., Flanagan, J.J., Hummel, T., Vasconcelos, M.L., Chess, A., and Zipursky, S.L. (2004). Analysis of Dscam diversity in regulating axon guidance in *Drosophila* mushroom bodies. Neuron *43*, 673–686.

Zhu, H., Hummel, T., Clemens, J.C., Berdnik, D., Zipursky, S.L., and Luo, L. (2006). Dendritic patterning by Dscam and synaptic partner matching in the Drosophila antennal lobe. Nat. Neurosci. *9*, 349–355.

Zlatic, M., Landgraf, M., and Bate, M. (2003). Genetic specification of axonal arbors: atonal regulates robo3 to position terminal branches in the *Drosophila* nervous system. Neuron *37*, 41–51.